Three-Dimensional Nonlinear Vibrations of Composite Beams – III. Chordwise Excitations

PERNGJIN F. PAI and ALI H. NAYFEH

Department of Engineering Science and Mechanics, Virginia Polytechnic Institute and State University, Blacksburg, Virginia 24061, U.S.A.

Abstract. Three nonlinear integro-differential equations of motion derived in Part I are used to investigate the forced nonlinear vibration of a symmetrically laminated graphite-epoxy composite beam. The analysis focuses on the case of primary resonance of the first in-plane flexural (chordwise) mode when its frequency is approximately twice the frequency of the first out-of-plane flexural-torsional (flapwise-torsional) mode. A combination of the fundamental-matrix method and the method of multiple scales is used to derive four first-order ordinary-differential equations describing the modulation of the amplitudes and phases of the interacting modes with damping, nonlinearity, and resonances. The eigenvalues of the Jacobian matrix of the modulation equations are used to determine the stability of their constant solutions, and Floquet theory is used to determine the stability and bifurcations of their limit-cycle solutions. Hopf bifurcations, symmetry-breaking bifurcations, period-multiplying sequences, and chaotic motions of the modulation equations are studied. The results show that the motion can be nonplanar although the input force is planar. Nonplanar responses may be periodic, periodically modulated, or chaotically modulated motions.

Key words: Autoparametric resonance, composite beams, chordwise excitations, chaos.

1. Introduction

For a slender, linearly elastic rod subject to a lateral harmonic excitation in one principal direction, Haight and King [1] investigated the effect of nonlinear inertia terms on the response of the first three modes by using an averaging method. They identified unstable regions in the planar response curves which correspond to parametrically excited nonplanar motions; they did not present quantitative results for the resulting nonplanar motions. From their experimental work, they concluded that the nonplanar motions are steady whirling motions with the point on the neutral axis tracing an elliptical path. Crespo de Silva and Glynn [2, 3] derived a consistent set of nonlinear equations governing the flexural-flexural-torsional vibration of isotropic beams. They showed that the generally neglected nonlinear terms arising from the curvature are of the same order as the nonlinear terms due to inertia and might have a significant influence on the response of the beam. In the analysis of large-amplitude out-of-plane oscillations of a thin circular ring, Maganty and Bickford [4] studied the case of a one-to-one internal resonance and found amplitude-modulated motions. Nayfeh, Mook, and Sridhar [5] and Sridhar, Nayfeh, and Mook [6] analyzed the nonlinear response of uniform hinged-clamped beams to primary- and secondary-resonant excitations, respectively. Nayfeh, Mook, and Lobitz [7] included the motion-induced stretching effect in the governing equations and studied the nonlinear response of nonuniform hinged-clamped beams to primary resonances. They showed that, in the case of modal interactions, if the high-frequency mode is directly excited, the response of the low-frequency mode could be very large due to an energy transfer to this mode from the high-frequency mode. But, if the low-frequency mode is directly excited, the response of the high-frequency mode is usually small. Elastic couplings among extensional, bending, and torsional stiffnesses are important

Nonlinear Dynamics **2**: 137–156, 1991
© 1991 *Kluwer Academic Publishers. Printed in the Netherlands.*

characteristics of composite structures. One well known example of taking advantage of the bending-twisting coupling effect is the X-29 demonstrator aircraft; the composite skin of its forward-swept wing has a built-in structural and aerodynamic stability.

In this paper, we show that a two-to-one internal resonance produced by bending-twisting couplings and nonlinear geometric couplings may lead the responses of a laminated composite beam subjected to harmonic chordwise excitations to nonplanar motions and the vibrations can be periodic, periodically modulated, or chaotically modulated.

2. Equations of Motion and Perturbation Solutions

The problem being studied is the forced vibration of the uniform, inextensional cantilever beam shown in Figure 1(a). The excitation is along the direction of the width of the cross section, which is called the chordwise direction. The equations of motion [8, 9] nondimensionalized using the length L of the beam and the characteristic time $L^2\sqrt{m/D_{33}}$ are

$$\ddot{v} + v^{iv} + \beta_{13}\gamma''' - j_3\ddot{v}'' = \varepsilon\Big\{-\mu_1\dot{v} - [v'(v'v'' + w'w'')']' - \beta_{11}(\gamma' w'')'$$
$$+ (\beta_{22} - 1)\Big[(\gamma w'' - \gamma^2 v'')' - w'''\int_0^s v''w'\,ds\Big]' - \frac{1}{2}\Big\{v'\int_1^s\Big[\int_0^s (v''^2 + w'^2)\,ds\Big]^{\cdot\cdot}\,ds\Big\}'$$
$$+ \beta_{13}(-v''w'' - \frac{1}{2}v'^2\gamma'' - w''^2\gamma + \frac{1}{2}\gamma^2\gamma'' + \gamma\gamma'^2)'\Big\}, \tag{1}$$

$$\ddot{w} + \beta_{22}w^{iv} - j_2\ddot{w}'' = \varepsilon\Big\{-\mu_2\dot{w} - \beta_{22}[w'(v'v'' + w'w'')']' + \beta_{11}(\gamma' v'')'$$
$$+ (\beta_{22} - 1)\Big[(\gamma v'' + \gamma^2 w'')' + v'''\int_0^s v'w''\,ds\Big]' - \frac{1}{2}\Big\{w'\int_1^s\Big[\int_0^s (v'^2 + w'^2)\,ds\Big]^{\cdot\cdot}\,ds\Big\}'$$
$$+ \beta_{13}\Big(-\gamma\gamma'' + \gamma v''w'' + v''^2 - \gamma^2 - \gamma''\int_0^s v'w''\,ds\Big)' + \hat{f}\Omega^2\cos\Omega t\Big\}, \tag{2}$$

$$j_1\ddot{\gamma} - \beta_{11}\gamma'' - \beta_{13}v''' = \varepsilon\Big\{-\mu_3\dot{\gamma} + (1 - \beta_{22})[(v''^2 - w''^2)\gamma - v''w'']$$
$$+ j_1\Big(\int_0^s v''w'\,ds\Big)^{\cdot\cdot} - j_1(\dot{v}'w')^{\cdot} + (j_2 - j_3)[\dot{v}'^2 - \dot{w}'^2)\gamma - \dot{w}'\dot{v}']$$
$$+ \beta_{13}\Big(w'''\gamma + w'''\int_0^s v'w''\,ds - \frac{1}{2}v'''\gamma^2 + \frac{1}{2}v'''v'^2 + v''^2v' + v'w''^2\Big)\Big\}. \tag{3}$$

The boundary conditions are

$$v = v' = w = w' = \gamma = 0 \quad \text{at } s = 0, \tag{4}$$

$$v'' = w'' = \gamma' = 0 \quad \text{at } s = 1, \tag{5a}$$

$$v''' + \beta_{13}\gamma'' - j_3\ddot{v}' = \varepsilon\Big[(\beta_{22} - 1)\Big(w'''\gamma - v'''\gamma^2 - w'''\int_0^1 v''w'\,ds\Big)$$
$$- v'(v'v''' + w'w''') + \frac{1}{2}\beta_{13}(\gamma^2\gamma'' - v'^2\gamma'')\Big] \quad \text{at } s = 1, \tag{5b}$$

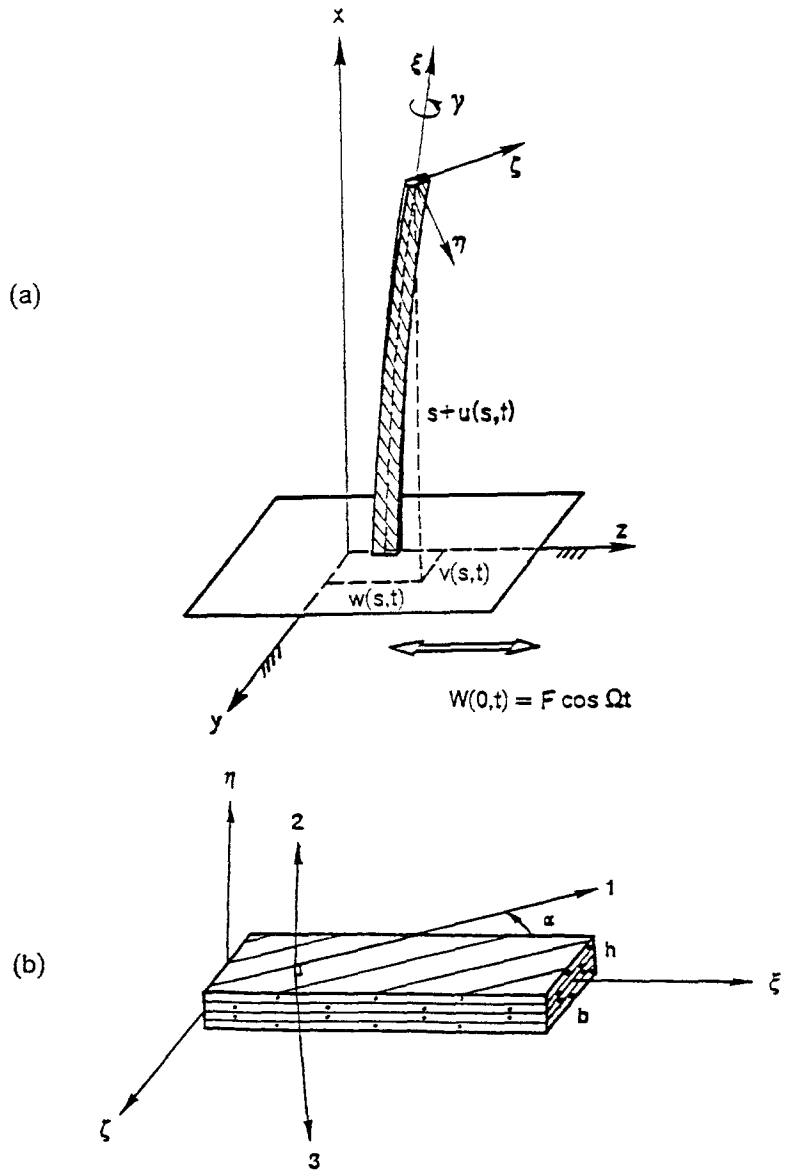

Fig. 1. Coordinate systems: (a) x-y-z = inertial reference frame, $\xi - \eta - \zeta$ = principal axes of the beam's cross-section at position s, (b) 1-2-3 = material coordinates.

$$\beta_{22}w''' - j_2\ddot{w}' = \varepsilon\Big[(\beta_{22}-1)\Big(v'''\gamma + w'''\gamma^2 + v'''\int_0^1 w''v'\,\mathrm{d}s\Big)$$

$$-\beta_{22}w'(v'v''' + w'w''') - \beta_{13}\Big(\gamma\gamma'' + \gamma''\int_0^1 w''v'\,\mathrm{d}s\Big)\Big] \quad \text{at } s = 1\,. \tag{5c}$$

Here, s is the distance from the origin of the x-y-z coordinate system to the undeformed position of the observed element, m is the mass per unit length of the beam, the prime denotes the derivative with respect to s, the dot denotes the derivative with respect to time t, γ is the twisting

angle about the ξ axis, and ε is a nondimensional parameter introduced for bookkeeping purposes. D_{11}, D_{22}, D_{33}, and D_{13} are the stiffnesses for torsion, bending of w, bending of v, and bending-twisting coupling, respectively. F is the excitation amplitude. Moreover, $\hat{f} = F/L$, $\beta_{11} = D_{11}/D_{33}$, $\beta_{22} = D_{22}/D_{33}$, $\beta_{13} = D_{13}/D_{33}$; j_1, j_2 and j_3 are the normalized rotary inertias; μ_1, μ_2, and μ_3 are the normalized damping coefficients. Equations (1)–(5) are the same as those in the second part of this paper except that the forcing term $\hat{f}\Omega^2 \cos \Omega t$ appears in the equation governing $w(s, t)$ instead of the equation governing $v(s, t)$.

To quantitatively describe the nearness of the autoparametric resonance, we introduce a detuning parameter δ defined by

$$\omega_2 = 2\omega_1(1 + \varepsilon\delta)\,, \tag{6}$$

where ω_2 is the natural frequency of the first in-plane flexural (chordwise) mode and ω_1 the natural frequency of the first out-of-plane flexural-torsional (flapwise-torsional) mode, and δ depends on b, the ply angles, and/or the stacking sequence. The nearness of the external resonance is represented by another detuning parameter σ defined by

$$\Omega = \omega_2(1 + \varepsilon\sigma)\,. \tag{7}$$

Following the same procedure used in Part II, we obtain the first-order asymptotic solution

$$v(s, t) = V(s)a_1(\varepsilon t)\cos\left(\frac{\Omega}{2}\, t - \frac{\nu_1 + \nu_2}{2}\right) + \ldots\,, \tag{8}$$

$$w(s, t) = W(s)a_2(\varepsilon t)\cos(\Omega t - \nu_2) + \ldots\,, \tag{9}$$

$$\gamma(s, t) = \Gamma(s)a_1(\varepsilon t)\cos\left(\frac{\Omega}{2}\, t - \frac{\nu_1 + \nu_2}{2}\right) + \ldots\,. \tag{10}$$

The equations governing the amplitudes a_i and phases ν_i are

$$a_1' + \hat{\mu}_1 a_1 + \Lambda_1 a_1 a_2 \sin \nu_1 = 0\,, \tag{11}$$

$$\frac{1}{2}\, a_1(\nu_1' + \nu_2') - (\sigma + \delta)\omega_1 a_1 + \Lambda_1 a_1 a_2 \cos \nu_1 + S_{11}a_1^3 + S_{12}a_1 a_2^2 = 0\,, \tag{12}$$

$$a_2' + \hat{\mu}_2 a_2 - \Lambda_2 a_1^2 \sin \nu_1 + \hat{R} \sin \nu_2 = 0\,, \tag{13}$$

$$a_2 \nu_2' - 2\omega_1 \sigma a_2 + \Lambda_2 a_1^2 \cos \nu_1 + S_{21}a_1^2 a_2 + S_{22}a_2^3 + \hat{R} \cos \nu_2 = 0\,, \tag{14}$$

where $\hat{\mu}_1$, $\hat{\mu}_2$, Λ_1, Λ_2, S_{11}, S_{12}, S_{21}, S_{22}, and $\hat{R}$ are defined in Appendix A,

$$\nu_1 = \theta_2 - 2\theta_1 + 2\omega_1 \delta T_1\,, \tag{15}$$

and

$$\nu_2 = \omega_2 \sigma T_1 - \theta_2\,. \tag{16}$$

Periodic solutions of the beam correspond to the fixed points (i.e., constant solutions) of (11)–(14), which in turn correspond to $a_1' = a_2' = \nu_1' = \nu_2' = 0$.

Introducing the Cartesian coordinates p_i and q_i defined by

$$p_1 = a_1 \cos\left(\frac{\nu_1 + \nu_2}{2}\right), \qquad q_1 = a_1 \sin\left(\frac{\nu_1 + \nu_2}{2}\right), \tag{17}$$

$$p_2 = a_2 \cos \nu_2, \qquad q_2 = a_2 \sin \nu_2, \tag{18}$$

into the averaged equations (11)–(14), we obtain

$$p_1' = -\hat{\mu}_1 p_1 - \omega_1(\sigma + \delta)q_1 - \Lambda_1(q_1 p_2 - q_2 p_1) + S_{12}(p_2^2 + q_2^2)q_1 + S_{11}(p_1^2 + q_1^2)q_1, \tag{19}$$

$$q_1' = -\hat{\mu}_1 q_1 + \omega_1(\sigma + \delta)p_1 - \Lambda_1(q_1 q_2 + p_2 p_1) - S_{12}(p_2^2 + q_2^2)p_1 - S_{11}(p_1^2 + q_1^2)p_1, \tag{20}$$

$$p_2' = -\hat{\mu}_2 p_2 - 2\omega_1 \sigma q_2 + 2\Lambda_2 p_1 q_1 + S_{21}(p_1^2 + q_1^2)q_2 + S_{22}(p_2^2 + q_2^2)q_2, \tag{21}$$

$$q_2' = -\hat{\mu}_2 q_2 + 2\omega_1 \sigma p_2 + \Lambda_2(q_1^2 - p_1^2) - S_{21}(p_1^2 + q_1^2)p_2 - S_{22}(p_2^2 + q_2^2)p_2 - \hat{R}. \tag{22}$$

3. Numerical Results

We study the case of primary resonance of the first mode of w in the presence of a two-to-one internal resonance between this mode and the first bending-twisting mode of v and γ. We assume that the damping coefficients are $\mu_1 = 0.07$, $\mu_2 = 0.13$, and $\mu_3 = 0.0003$, which are obtained by assuming that the modal damping ratios of v, w, and γ are 0.01, 0.01, and 0.03, respectively. For all the response curves presented in this paper, we use solid lines to denote stable solutions, dashed lines to denote unstable solutions with at least one eigenvalue being positive, and dotted lines to denote unstable solutions with a pair of complex conjugate eigenvalues having a positive real part.

When the excitation amplitude $f \equiv \hat{f}\int_0^1 W \, ds = 0.01$, Figures 2(a) and (b) show the frequency-response curves for the cases where the internal-detuning parameter δ is -0.11 and -0.093, respectively. When δ is a large negative number, the two flexural modes are greatly detuned and the out-of-plane response curve (i.e., a_1) consists of one branch around the point $\sigma = -\delta$, which is the resonant condition of $v(s, t)$. When δ is increased to -0.093, a second branch appears in the out-of-plane response curve, as shown in Figure 2(b). As δ is increased to 0.05, the two branches of the nonplanar response curve merge, as shown in Figure 3(a). The fixed-point solution loses its stability through a Hopf bifurcation at $\sigma = \sigma_1 = -0.00725$ and $\sigma = \sigma_2 = 0.033588$, and amplitude- and phase-modulated motions are expected in the interval $\sigma_1 < \sigma < \sigma_2$. We note that the out-of-plane motion is excited through the autoparametric resonance. The amplitude a_2 of planar response corresponds essentially to the linear solution because the amplitude of the base motion is small and the bending stiffness in the z-direction is large. The variation of the phase ν_2 with σ shown in Figure 3(b) also confirms the linearity of the chordwise planar vibration because the phase angle changes from 0° to 180° around the resonant point $\sigma = 0$. Furthermore, for nonplanar motions, the amplitude a_2 of the directly excited mode is much smaller than the amplitude a_1 of the indirectly excited mode through the autoparametric resonance. It indicates that most of the input energy is spilled over into the lower mode.

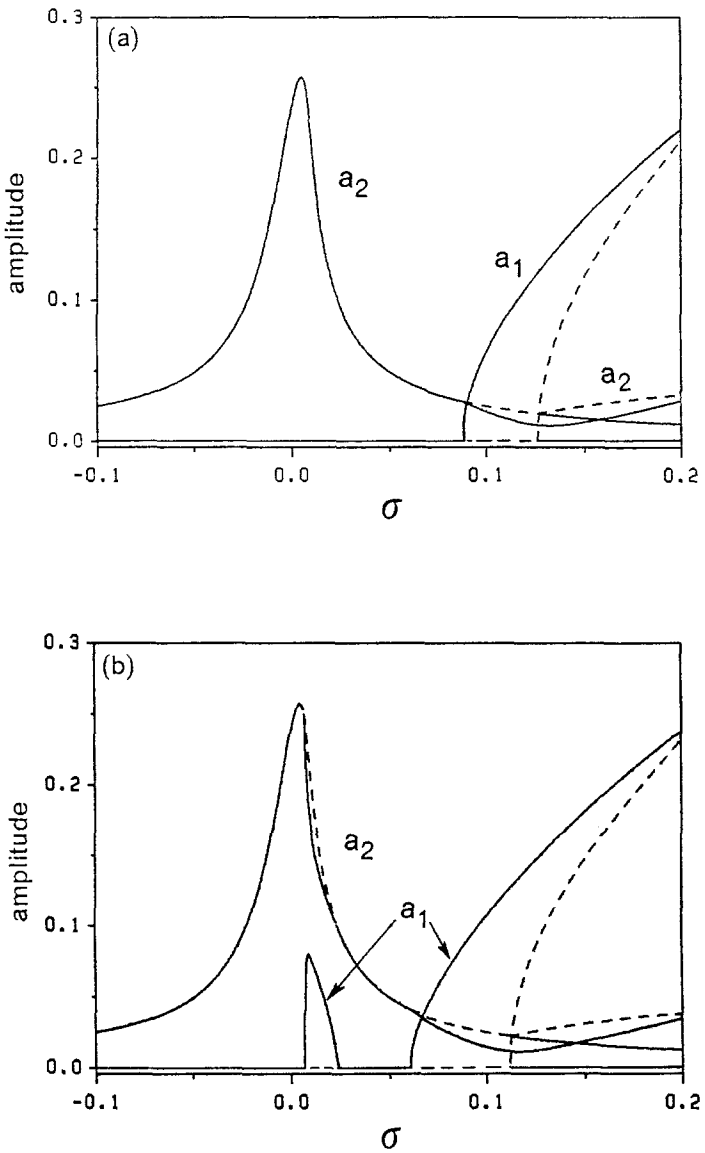

Fig. 2. Frequency-response curves: (a) $\delta = -0.11$, (b) $\delta = -0.093$.

In Figures 4 and 5, we show representative force-response curves. Figure 4 shows representative curves [10] for $\chi < 0$, where $\chi = 2\sigma\omega_1^2(\sigma + \delta) - \hat{\mu}_1\hat{\mu}_2$, and Figure 5 shows representative curves for $\chi > 0$. Figure 4(b) shows that, without the cubic terms, the amplitude a_2 of the in-plane mode saturates when the forcing amplitude increases beyond the threshold value f_1; the extra energy is spilled over into the lower mode. However, Figure 4(a) shows that the cubic terms reduce the threshold value of f_1 for the onset of out-of-plane motions, destabilize some nonplanar periodic motions by producing amplitude- and phase-modulated motions, and reduce the amplitude of the directly excited mode when the input force increases beyond the threshold value f_1. Furthermore, for large levels of excitation, a second branch of out-of-plane motions is produced

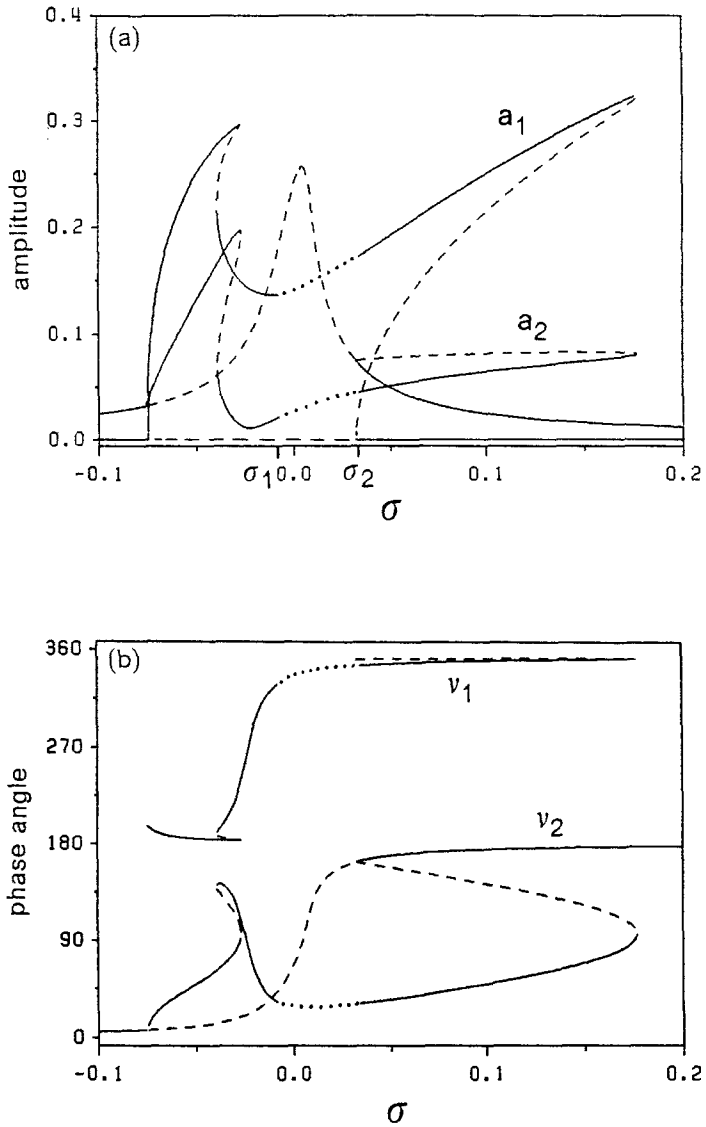

Fig. 3. (a) Frequency-response curves and (b) phase angles: $\delta = 0.05$.

by the cubic terms. In addition to the saturation phenomenon, Figure 5(b) exhibits jumps at f_2 and f_3. Again, Figure 5(a) shows that the cubic terms reduce the threshold value for the onset of out-of-plane motions, destabilize some nonplanar periodic motions by producing amplitude- and phase-modulated motions, and reduce the amplitude of the directly excited mode when the input force increases beyond f_3. We note that $f = f_3$ is a subcritical (reverse) pitchfork bifurcation point at which one of the real eigenvalues of the Jacobian matrix of equations (19)–(22) changes sign and there is a change in the number of fixed points. At $f = f_2$, a saddle-node bifurcation occurs, which is accompanied by a change in the number of fixed points. For $f_2 < f < f_3$, there are three possible solutions: a stable planar solution, a stable nonplanar solution, and an unstable nonplanar solution. The response of the beam will depend on the initial conditions. When $f > f_3$, the

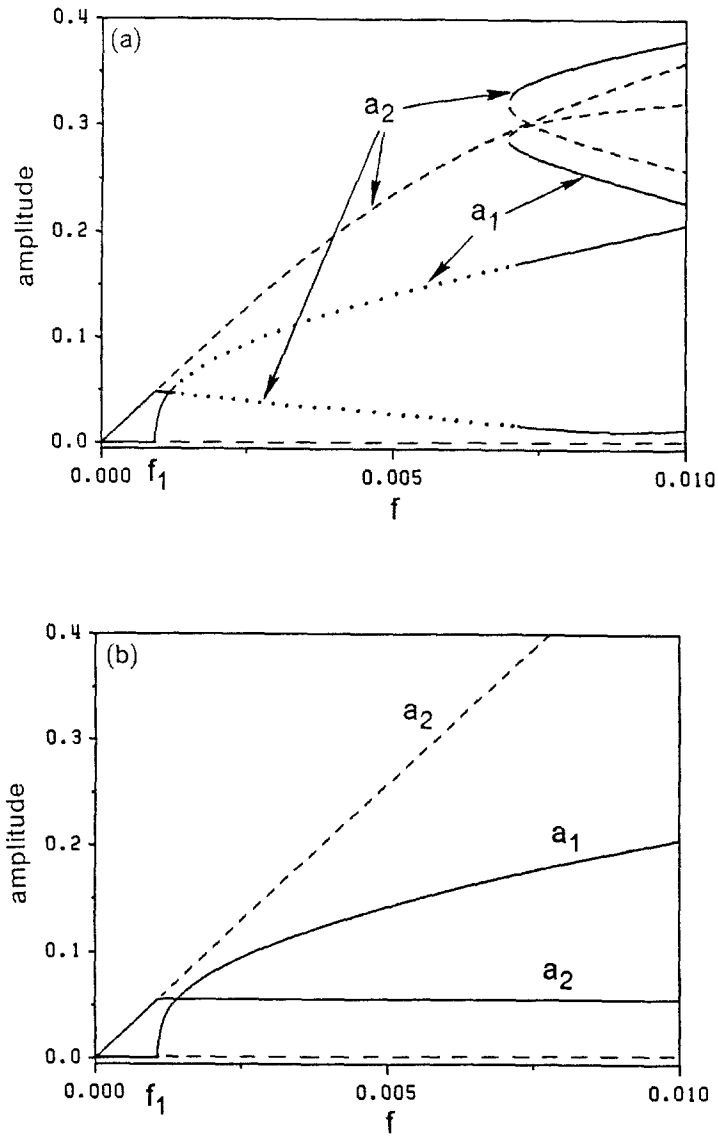

Fig. 4. Force-response curves obtained by (a) including the cubic terms and (b) neglecting the cubic terms: $\delta = 0.05$, $\sigma = 0.0$.

response is nonplanar whereas when $f < f_2$ the response is a planar flexural vibration, which is linear.

Changing the damping coefficient by a ratio R_{atio}, the locations of the Hopf bifurcation points change, as shown in Figure 6. We note that increasing the damping coefficients may suppress chaotic motions. Increasing the damping coefficients above critical values results in the elimination of the Hopf bifurcations and hence amplitude- and phase-modulated motions.

Inspecting the modulation equations (19)–(22), we note that they are invariant under the transformation $(p_1, q_1, p_2, q_2) \rightarrow (-p_1, -q_1, p_2, q_2)$. Thus, there is an inversion symmetry in the responses of $v(s, t)$ and $\gamma(s, t)$. Because $w(s, t)$ is externally excited, it does not possess an inversion symmetry and the phase angle ν_2 between the input force and $w(s, t)$ is unique.

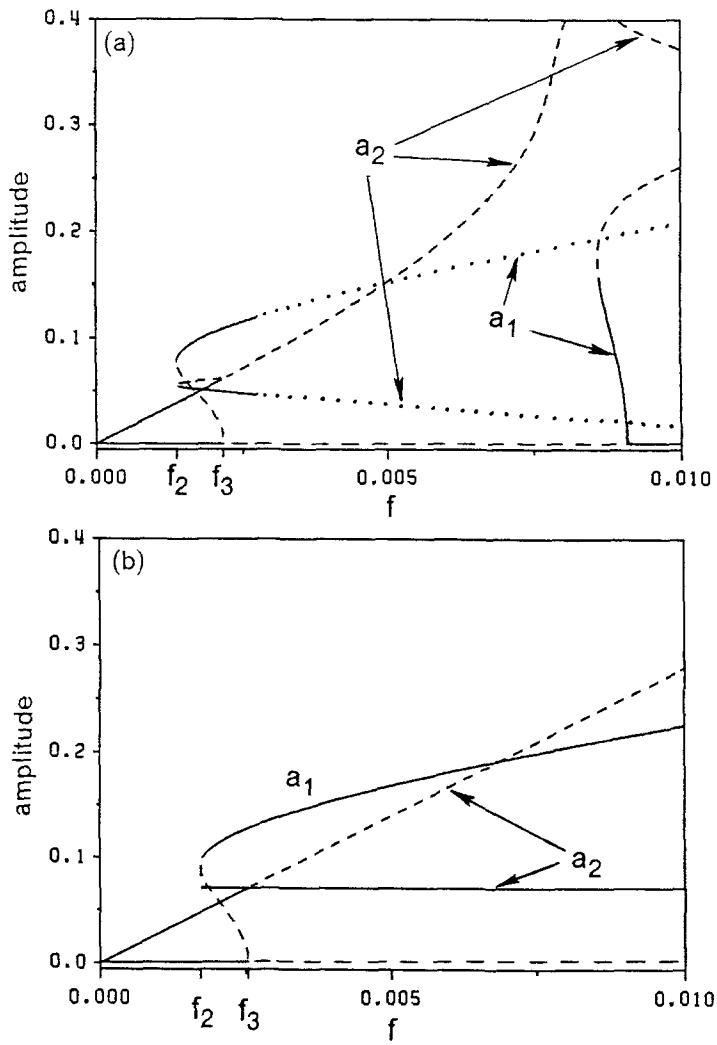

Fig. 5. Force-response curves obtained by (a) including the cubic terms and (b) neglecting the cubic terms: $\delta = 0.05$, $\sigma = 0.015$.

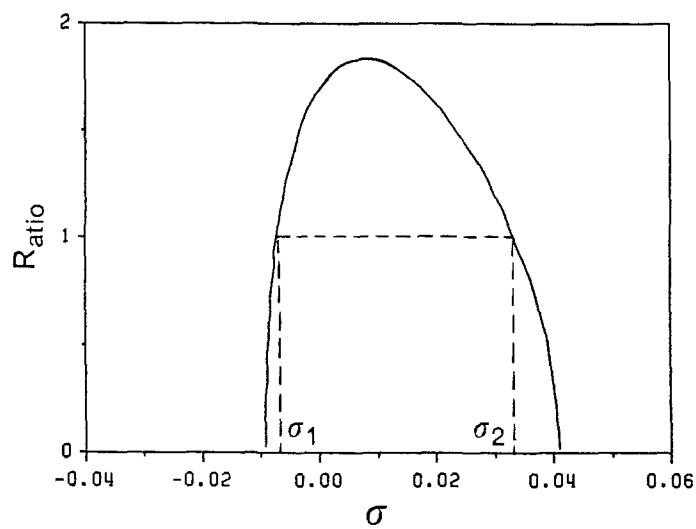

Fig. 6. The influence of damping on the location of the Hopf bifurcation points: $\delta = 0.05$, μ_1, μ_2, $\mu_3 = R_{atio} \times (0.07, 0.13, 0.0003)$.

Using the method proposed by Chua and Lin [11], we studied amplitude- and phase-modulated motions for fifty different input frequencies and obtained Figure 7, which shows the periods and the maxima and minima of the amplitudes of the calculated limit cycles. In Figure 7(b), we use dotted lines to denote the maxima and minima of the amplitudes of chaotic attractors.

Figures 8(a)–(n) show representative solutions existing between the Hopf bifurcation points σ_1 and σ_2. On the right-hand side is the power spectral density of p_1. As σ increases beyond σ_1 a small limit cycle, which is symmetric with respect to the unstable fixed-point solution, is born, indicating that $\sigma = \sigma_1$ is a supercritical Hopf bifurcation point. One of the Floquet multipliers

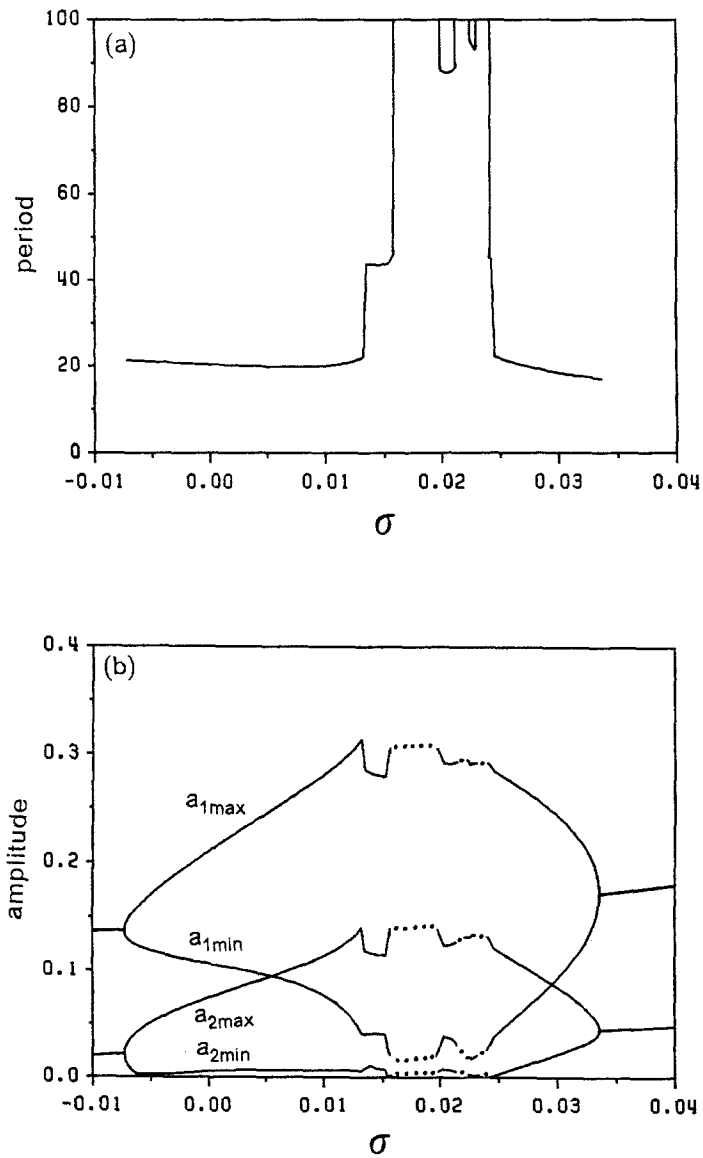

Fig. 7. (a) Period of the amplitude and phase modulations and (b) the maxima and minima of amplitudes: $\delta = 0.05$.

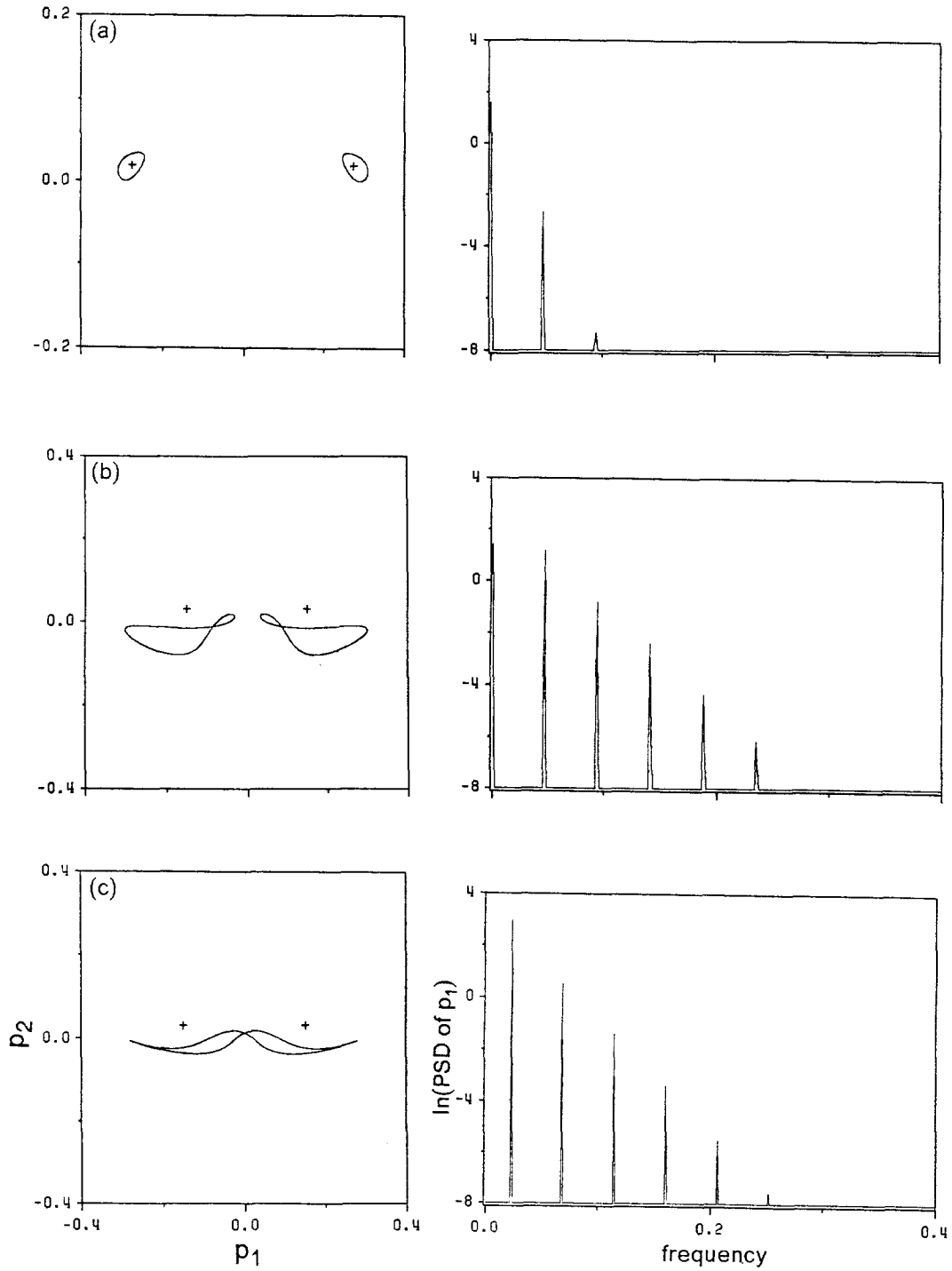

Fig. 8. The two-dimensional projection of the attractor onto the $p_1 - p_2$ plane and the PSD (power spectral density) of p_1 when $\delta = 0.05$: (a) $\sigma = -0.0062857$, (b) $\sigma = 0.012572$, (c) $\sigma = 0.015143$, (d) $\sigma = 0.015658$, (e) $\sigma = 0.015879$, (f) $\sigma = 0.019638$, (g) $\sigma = 0.020286$, (h) $\sigma = 0.02205$, (i) $\sigma = 0.022734$. (j) $\sigma = 0.023584$, (k) $\sigma = 0.023617$, (l) $\sigma = 0.02381$, (m) $\sigma = 0.02406$, and (n) $\sigma = 0.028857$ (+ denotes the unstable fixed-point solutions).

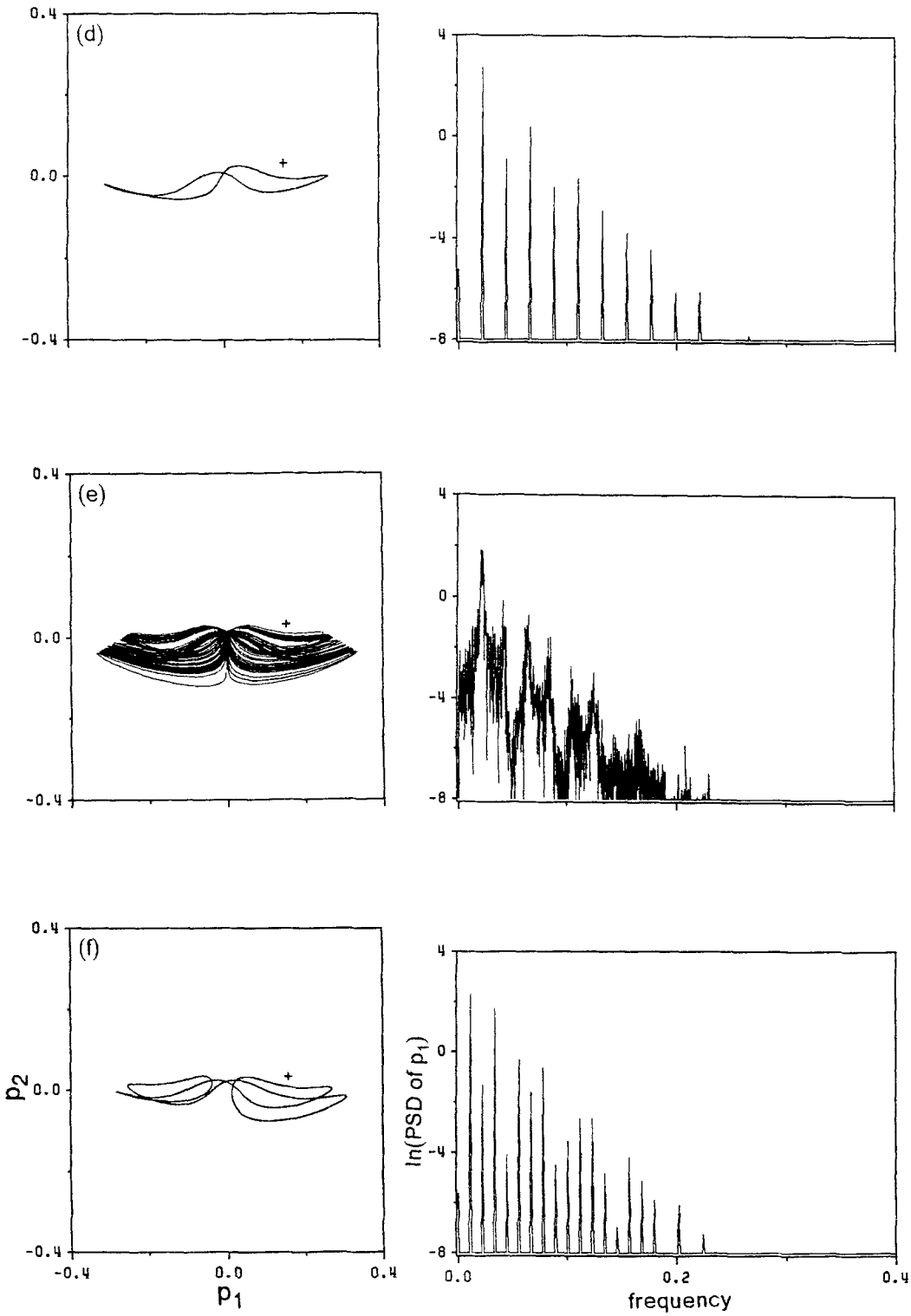

Fig. 8. (continued).

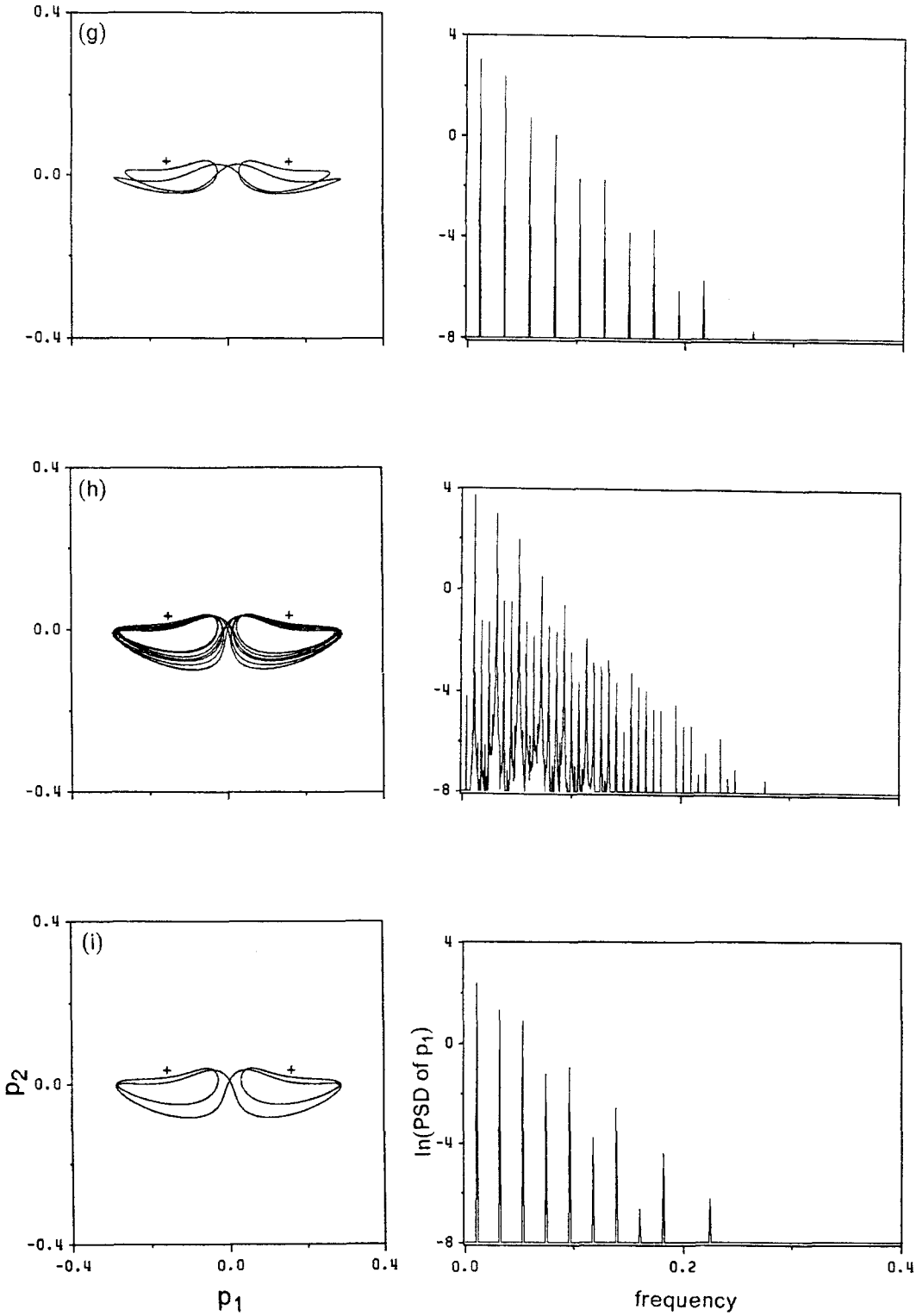

Fig. 8. (continued).

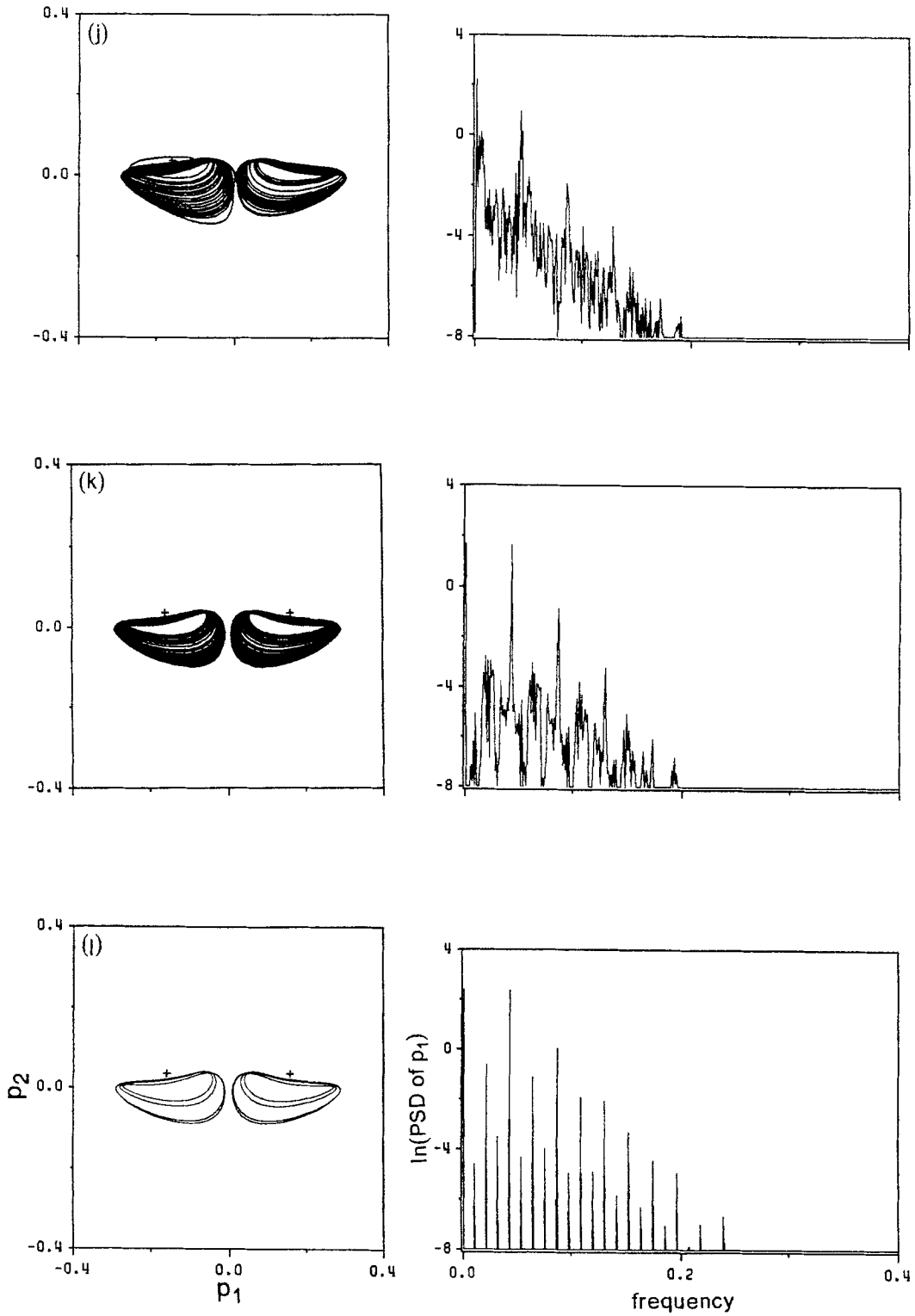

Fig. 8. (continued).

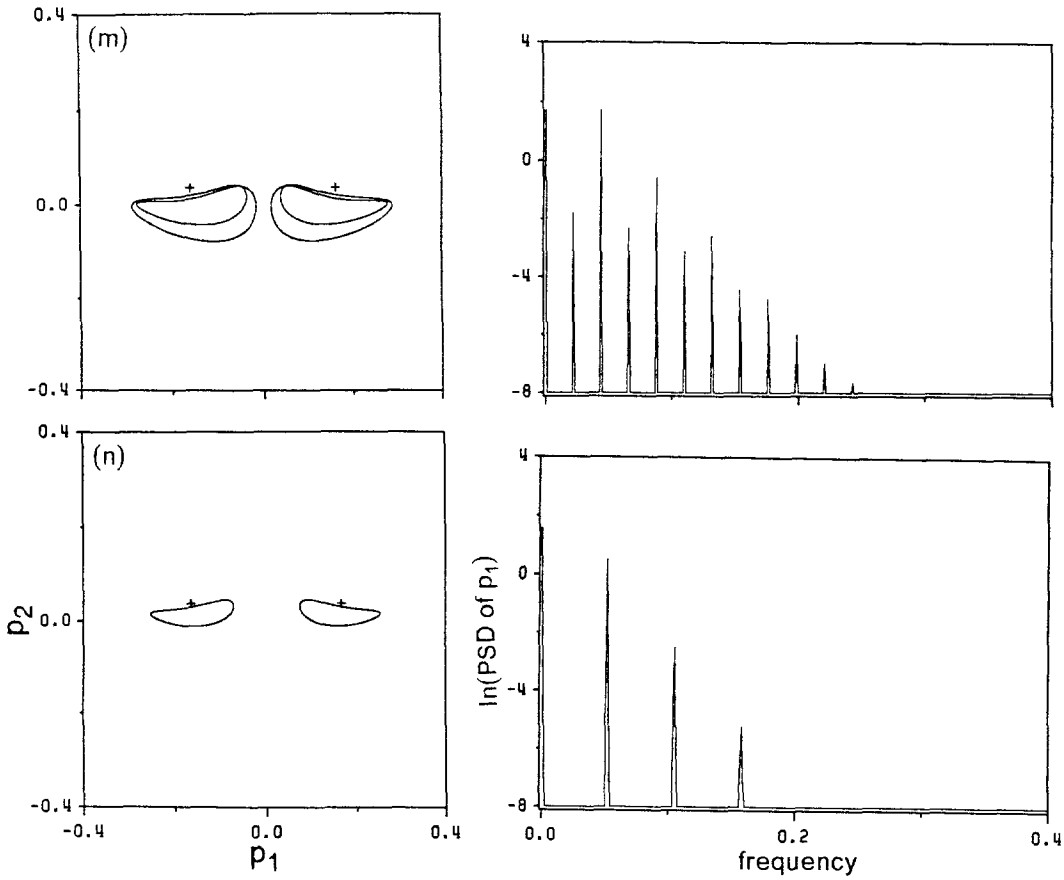

Fig. 8. (continued).

leaves the unit circle in the complex plane through +1, indicating a symmetry-breaking bifurcation, at a value of σ not far away from σ_1, as shown in Figure 8(a); the two plus signs indicate a pair of unstable fixed-point solutions. Figure 8(b) shows a pair of asymmetric attractors, which coexist in the interval $0.011457 < \sigma < 0.013226$. Then, these two attractors merge and become a symmetric attractor with respect to $p_1 = 0$, as shown in Figure 8(c). When σ increases to 0.015658, the attractor loses its symmetry, as shown in Figure 8(d). As σ increases further, the attractor suffers from a cyclic-fold bifurcation and becomes chaotic in the interval $0.015658 < \sigma < 0.019638$; Figure 8(e) shows the chaotic attractor at $\sigma = 0.015879$. Its Lyapunov exponents l_i are 0.00626, 0.0, −0.0963, and −0.111 and its dimension is 2.065, which is fractal. The Lyapunov exponents l_i were calculated by using the algorithm of Wolf *et al.* [12]. We note that the sum of the Lyapunov exponents is $\Sigma_{i=1}^{4} l_i = -2(\hat{\mu}_1 + \hat{\mu}_2) = -0.2004$, as it should. At $\sigma = 0.019638$, the attractor becomes periodic, as shown in Figure 8(f). When $0.019638 < \sigma < 0.022955$, the attractor undergoes a sequence of period-doubling bifurcations, culminating in chaos; then it undergoes a sequence of reverse period-doubling bifurcations, as shown in Figures 8(g)–(i). Although attractor 8(h) looks like a large-period limit cycle, it cannot be located by the shooting technique. Moreover, its Lyapunov exponents (0.000957, 0.0, −0.0866, −0.115) and its dimension 2.011 show that it is chaotic. When $\sigma > 0.022955$, the attractor becomes chaotic as shown Figure 8(j). It is a Lorenz type chaotic attractor since it wanders about the two unstable fixed-point solutions; it has the

Lyapunov exponents 0.0238, 0.0, −0.107, −0.117 and the fractal dimension 2.222. Increasing σ slightly, we find that the chaotic attractor splits into two, as shown in Figure 8(k), each of them wanders about one of the fixed-point solutions. They are of the Rossler type and have the Lyapunov exponents 0.0180, 0.0, −0.108, −0.110 and the fractal dimension 2.166. As σ increases further, these two attractors become periodic and undergo a sequence of reverse period-doubling bifurcations, as shown in Figures 8(l)–(n). When σ increases beyond σ_2(=0.033588), the small limit-cycle symmetric attractor becomes a point attractor.

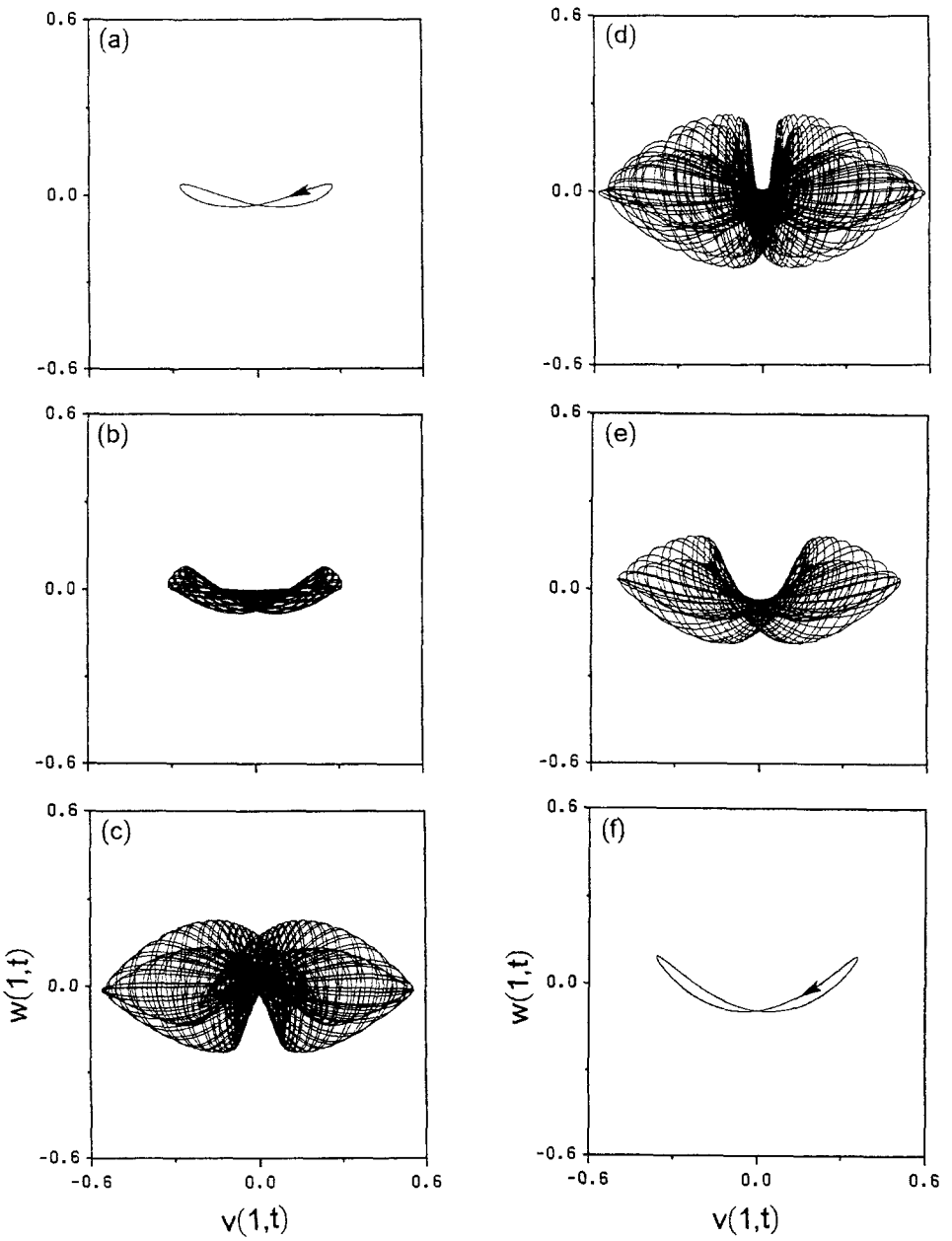

Fig. 9. The path of the tip of the beam when $\delta = 0.05$: (a) $\sigma = -0.01$, (b) $\sigma = -0.0062857$, (c) $\sigma = 0.015143$, (d) $\sigma = 0.02406$, (e) $\sigma = 0.028857$, and (f) $\sigma = 0.04$.

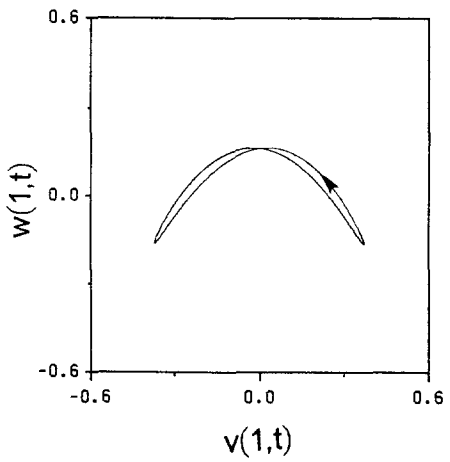

Fig. 10. The path of the tip of the beam: $\delta = 0.05$ and $\sigma = -0.064548$.

Figures 9(a) and (f) show the periodic tip motion for $\sigma = -0.01 < \sigma_1$ and $\sigma = 0.04 > \sigma_2$, respectively. The periodic responses are stationary and appear as a "figure eight" since the period of one mode is exactly twice that of the other mode. Figures 9(b)–(e) show the trajectories of the tip of the beam, corresponding to the amplitude- and phase-modulated motions shown in Figures 8(a), (c), (m), and (n). The "figure-eight" response evolves continuously because the two modes are continuously exchanging energy.

Checking the tip motion corresponding to the left branch of the nonplanar response curve in Figure 3(a), we find that the path of the tip is curved downward, as shown in Figure 10. It can be seen by considering the bending-twisting coupling that this motion needs less energy for its excitation than the one curved upward.

4. Conclusions

An analysis is presented of the nonlinear response of a symmetrically laminated graphite-epoxy composite beam to a chordwise excitation. The analysis focuses on the case of primary resonance of the first flexural mode along the chord direction when its frequency is approximately twice the frequency of the first out-of-plane flexural-torsional mode. A combination of the fundamental-matrix method and the method of multiple scales is used to derive four first-order ordinary-differential equations describing the modulation of the amplitudes and phases of the interacting modes. The eigenvalues of the Jacobian matrix of the modulation equations are used to determine the stability and bifurcations of their constant solutions, and Floquet theory is used to determine the stability and bifurcations of their limit-cycle solutions. Hopf bifurcations, symmetry-breaking bifurcations, period-multiplying sequences, and chaotic motions of the modulation equations are studied.

The results show that the motion can be planar and/or nonplanar although the input force is planar, and the steady response depends on their basins of attraction. Nonplanar responses may be periodic, periodically modulated, or chaotically modulated motions.

In the absence of the cubic nonlinear terms, the directly excited flexural mode saturates when

the input force exceeds a threshold value. However, including the cubic nonlinear terms eliminates the saturation phenomenon and destabilizes nonplanar motions through a Hopf bifurcation. Between the Hopf bifurcation points, the response is either a periodically or a chaotically modulation motion. We found two routes to chaos: a cyclic-fold bifurcation and a sequence of period-doubling bifurcations.

Acknowledgement

This work was supported by the Army Research Office Grant No. DAAL03-89-K-0180 and the Air Force Office of Scientific Research under Grant No. F49620-87-C-0088.

Appendix A: Coefficients for Equations (11)–(14)

$$\hat{\mu}_1 = R_2/R_1 \ (=0.035230)$$

$$\Lambda_1 = R_3/R_1 \ (=3.0908)$$

$$S_{12} = -R_4/R_1 \ (=7.7105)$$

$$S_{11} = -R_5/R_1 \ (=4.3686)$$

$$\hat{\mu}_2 = E_2/E_1 \ (=0.065002)$$

$$\Lambda_2 = -E_3/E_1 \ (=0.77311)$$

$$S_{21} = -E_4/E_1 \ (=1.6597)$$

$$S_{22} = -E_5/E_1 \ (=0.51760)$$

$$\hat{R} = -2\hat{f}\omega_1^2 \int_0^1 W \, \mathrm{d}s/E_1$$

where

$$R_1 = \omega_1 \int_0^1 (j_1\Gamma^2 + V^2 - j_3 V''V) \, \mathrm{d}s$$

$$R_2 = \frac{1}{2}\,\omega_1 \int_0^1 (\mu_3\Gamma^2 + \mu_1 V^2) \, \mathrm{d}s$$

$$R_3 = \frac{1}{4}\int_0^1 \Big[(1-\beta_{22})V''W''\Gamma - \beta_{13}W'''\Gamma^2 + j_1\omega_1^2\Big(\Gamma\int_0^s V''W' \, \mathrm{d}s + V'W'\Gamma\Big)$$
$$+ 2(j_2 - j_3)\omega_1^2 V'W'\Gamma + \beta_{11}(W''\Gamma')'V + (1-\beta_{22})(W''\Gamma)''V + \beta_{13}(V''W'')'V\Big] \mathrm{d}s$$
$$+ \frac{1}{4}\,[(\beta_{22}-1)VW'''\Gamma]^{s=1}$$

$$R_4 = \frac{1}{4}\int_0^1 \Big[(\beta_{22}-1)W''^2\Gamma^2 + \beta_{13}\Gamma W'''\int_0^s V'W''\,\mathrm{d}s + \beta_{13}V'W''^2\Gamma$$
$$- 4(j_2-j_3)\omega_1^2 W'^2\Gamma^2 + (1-\beta_{22})V\Big(W'''\int_0^s V''W'\,\mathrm{d}s\Big)' - (V'(W'W'')')'V$$
$$- \beta_{13}V(W''^2\Gamma)'\Big)\,\mathrm{d}s$$
$$+ \frac{1}{4}\Big[(\beta_{22}-1)VW'''\int_0^1 V''W'\,\mathrm{d}s + VV'W'W'''\Big]^{s=1}$$

$$R_5 = \frac{1}{16}\int_0^1 \Big[6(1-\beta_{22})V''^2\Gamma^2 + \beta_{13}(-3V'''\Gamma^3 + 3V'''V'^2\Gamma + 6V''^2V'\Gamma)$$
$$+ 2(j_2-j_3)\omega_1^2 V'^2\Gamma^2 + 6(1-\beta_{22})V(V''\Gamma^2)'' - 6V(V'(V'V'')')'$$
$$+ \beta_{13}(-3V(V'^2\Gamma'')' + 3V(\Gamma^2\Gamma'')' + 6V(\Gamma\Gamma'^2)') + 4\omega_1^2 V\Big(V'\int_1^s\int_0^s V'V'\,\mathrm{d}s\,\mathrm{d}s\Big)'\Big]\,\mathrm{d}s$$
$$- \frac{3}{8}\Big[(1-\beta_{22})VV'''\Gamma^2 - VV'^2V''' - \frac{1}{2}\beta_{13}VV'^2\Gamma'' + \frac{1}{2}\beta_{13}V\Gamma^2\Gamma'''\Big]^{s=1}$$

$$E_1 = 2\omega_1\int_0^1 (W^2 - j_2WW'')\,\mathrm{d}s$$

$$E_2 = \mu_2\omega_1\int_0^1 W^2\,\mathrm{d}s$$

$$E_3 = \frac{1}{4}\int_0^1 [\beta_{11}W(V''\Gamma')' + (\beta_{22}-1)W(V''\Gamma)'' + \beta_{13}(-W(\Gamma\Gamma'')' + W(V''^2)' - W(\Gamma'^2)')]\,\mathrm{d}s$$
$$- \frac{1}{4}[(\beta_{22}-1)WV'''\Gamma - \beta_{13}W\Gamma\Gamma'']^{s=1}$$

$$E_4 = \frac{1}{4}\int_0^1 \Big[(\beta_{22}-1)(W(W''\Gamma^2)'' + W\Big(V'''\int_0^s V'W''\,\mathrm{d}s)'\Big) - \beta_{22}W(W'(V'V'')')'$$
$$+ \beta_{13}(W(\Gamma V''W'')' - W\Big(\Gamma''\int_0^s V'W''\,\mathrm{d}s)'\Big)\Big]\,\mathrm{d}s$$
$$- \frac{1}{4}\Big[(\beta_{22}-1)W\Big(W'''\Gamma^2 + V'''\int_0^1 W''V'\,\mathrm{d}s\Big) - \beta_{22}WW'V'V''' - \beta_{13}W\Gamma''\int_0^1 W''V'\,\mathrm{d}s\Big]^{s=1}$$

$$E_5 = \int_0^1 \Big[-\frac{3}{8}\beta_{22}W(W'(W'W'')')' + \omega_1^2 W\Big(W'\int_1^s\int_0^s W'^2\,\mathrm{d}s\,\mathrm{d}s\Big)'\Big]\,\mathrm{d}s + \frac{3}{8}\beta_{22}[WW'^2W''']^{s=1}.$$

References

1. Haight, E. C. and King, W. W., 'Stability of nonlinear oscillations of an elastic rod', *The Journal of the Acoustical Society of America* **52**, 1972, 899–911.
2. Crespo da Silva, M. R. M. and Glynn, C. C., 'Nonlinear flexural-flexural-torsional dynamics of inextensional beams – I. Equations of motion', *Journal of Structural Mechanics* **6**, 1978, 437–448.
3. Crespo da Silva, M. R. M. and Glynn, C. C., 'Nonlinear flexural-flexural-torsional dynamics of inextensional beams – II. Forced motions', *Journal of Structural Mechanics* **6**, 1978, 449–461.

4. Maganty, S. P. and Bickford, W. B., 'Large amplitude oscillations of thin circular rings', *Journal of Applied Mechanics* **54**, 1987, 315–322.
5. Nayfeh, A. H., Mook, D. T., and Sridhar, S., 'Nonlinear analysis of the forced response of structural elements', *Journal of Acoustical Society of America* **55**, 1974, 281–291.
6. Sridhar, S., Nayfeh, A. H., and Mook, D. T., 'Nonlinear resonances in a class of multi-degree-of-freedom systems', *Journal of Acoustical Society of America* **58**, 1975, 113–123.
7. Nayfeh, A. H., Mook, D. T., and Lobitz, D. W., 'Numerical-perturbation method for the nonlinear analysis of structural vibrations', *AIAA Journal* **12**, 1974, 1222–1228.
8. Pai, P. F. and Nayfeh, A. H., 'Three-dimensional nonlinear vibrations of composite beams – I. Equations of motion', *Nonlinear Dynamics* **1**, 1990, 477–502.
9. Pai, P. F. and Nayfeh, A. H., 'Three-dimensional nonlinear vibrations of composite beams – II. Flapwise excitations', *Nonlinear Dynamics* **2**, 1991, 1–34.
10. Nayfeh, A. H. and Mook, D. T., *Nonlinear Oscillations*, Wiley-Interscience, New York, 1979.
11. Chua, L. O. and Lin, P. M., *Computer-Aided Analysis of Electronic Circuits*, Prentice-Hall, Englewood Cliffs, N.J., 1975.
12. Wolf, A., Swift, J. B. Swinney, H. L., and Vastano, J. A., 'Determining Lyapunov exponents from a time series', *Physica D* **16**, 1985, 285–317.